Verfahrenstechnik auf einem neuen Level? It takes #HumanChemistry

Wir suchen kreative Ingenieurinnen und Ingenieure, die mit uns gemeinsam neue Wege gehen wollen – mit Fachwissen, Unternehmertum und Kreativität für innovative Lösungen. Informieren Sie sich unter:

evonik.de/karriere

EVONIK
Leading Beyond Chemistry

Almuth D. Schwarz[1,*]

Julian Dutzi[1]

Patrick Weber[2]

Carsten Sattler[2]

Karsten Schulz[2]

Thomas Caesar[2]

Jörg Meyer[1]

Achim Dittler[1]

Humidity Considerations in Filter Testing Based on Analysis of Filters from Gas Turbine Applications

Depth filters used in multistage filter systems adeptly clean the intake air of gas turbines, preventing damage and increasing performance. However, estimation of their service life is based on empirical data and/or standardized testing procedures, e.g., ISO 16890. By applying standardized synthetic test dusts at constant reference humidity, these testing procedures do not reflect application-typical loading conditions. Based on a direct comparison with field data, the influence of temporary exposure to high relative humidity on differential pressure and particle deposit structure is investigated. The results indicate that simulating humidity variations of the ambient atmosphere during filter tests leads to particle deposits, which more accurately reflect the actual behavior during operation.

Supporting Information available online

1 Introduction

Gas turbines are highly susceptible to damage when they are not adequately protected from particle exposure. To achieve a specific intake air quality, multistage depth filter systems composed of a series of pocket filters and cassette filters are applied. The primary performance characteristics of these filter elements can be described by tests according to ISO 29461 with reference to ISO 16890 in the case of coarse and fine filter grades as well as ISO 29463 (corresponding to EN1822:2011) for (H)EPA filter stages [1–3]. Depending on site-specific operating conditions and environmental circumstances, different grades of air filters are combined in progressive order to optimize the overall plant performance as well as the performance of the filter system itself with respect to filtration efficiency and differential pressure (Δp)[1]. A filter sequence is commonly comprised of two to three filter stages.

The first filter stage is exposed to the site-specific ambient aerosol and the subsequent filter stages to a remaining fraction of that same aerosol passing through the upfront filter stage. Although subject to local and temporal change, the particles in the ambient air are typically described by a bimodal mass-related particle size distribution (PSD). It can be divided into a fine fraction with a local maximum at $\approx 0.4\,\mu m$ and a coarse fraction above $1\,\mu m$ with a local maximum at $\approx 10\,\mu m$ [4]. In addition, there is a nuclei mode under $100\,nm$, which is not relevant in terms of mass distribution. While the coarse fraction is mainly removed by the first filter stage (referred to as pre-fil-

ter), the second and third stage are necessary to efficiently remove the fine fraction [5].

Several common synthetic test dusts, differentiated by chemical and physical properties, such as test dust L2 from ISO 15957, are used to determine dust holding capacities at defined Δp, e.g., 200 Pa or 300 Pa depending on the separation efficiency of the filter according to ISO 16890 [6]. These test dusts usually contain particle fractions and substances that differ greatly from typical ambient aerosols with respect to chemical composition and PSD. Especially the predominant aerosol in the second and third filter stage with a finer PSD is poorly represented [5].

One of the most important characteristics of each filter stage is its service life, which marks its required filter replacement. A reliable service life prediction enables the reduction of operating costs and resource consumption by optimizing maintenance and replacement activities. The service life is usually determined by an acceptable final Δp at given operating face velocity. Based on empirical knowhow, a correlation factor is applied to the dust holding capacity gained in lab tests. The correlation factors depend on the filter medium and design

[1]Almuth D. Schwarz, Julian Dutzi, Dr.-Ing. Jörg Meyer, Prof. Dr.-Ing. habil. Achim Dittler
almuth.schwarz@kit.edu
Karlsruhe Institute of Technology, Institute of Mechanical Process Engineering and Mechanics, Strasse am Forum 8, 76131 Karlsruhe, Germany.

[2]Patrick Weber, Carsten Sattler, Karsten Schulz, Dr.-Ing. Thomas Caesar
Freudenberg Filtration Technologies SE & Co. KG, Hoehnerweg 2–4, 69469 Weinheim, Germany.

1)   List of symbols at the end of the paper.

and are proprietary company information. Therefore, they vary greatly between different filters and filter types, and between suppliers.

The efficiency and service life of each filter stage are significantly influenced by several factors, including variations in ambient conditions. Relative humidity (RH) has previously been identified as a factor that influences the dust holding capacity of filters. Gupta et al. and Joubert et al. loaded HEPA filters with submicron and micron hygroscopic NaCl particles and nonhygroscopic Al_2O_3 at RH up to 90 % and 100 %, respectively, up to cake formation [7–9]. They found that a higher operating RH correlates with an increase in the filter dust holding capacity. Results by Ribeyre et al. from experiments with nanosized Al–Zn, C, and SiO_2 on sintered plates at RH up to 85 % support these findings [10].

Miguel, Montgomery et al., and Pei et al. observed an increasing dust holding capacity also prior to cake filtration with hygroscopic and nonhygroscopic submicron particles on various depth filter materials [11–14]. Current testing standards specify a constant RH of, e.g., 45 ± 10 % according to ISO 16890 during testing, in order to prevent deliquescence and condensation. The need of revising current filter testing standards by including the filters' operating temperature and RH was previously stated by Wilcox et al. and Pei et al. [15, 16].

Ongoing standardization activities consider the mentioned effects at least to some extent (ISO 29461–7). Especially moisture, which includes both water as evaporated matter (humidity) and liquid disperse matter (droplets), dramatically affects particle deposits. Wilcox et al. [15] suggest a test procedure of six individual tests. One test showed that the efficiency of salt-laden air filters declines after exposure to RH > 95 %. The structural change of deposits and its influences on the separation efficiency and Δp of the filters was not investigated.

In this paper, the influence of variations in RH on the particle deposits, Δp, and fractional separation efficiency is investigated. Laboratory experiments are carried out with soluble potassium chloride (KCl) particles, whose PSD is tailored to the second and third filter stage of gas turbines. A comparison to analyzed field data allows an assessment of the results and shows discrepancies between current testing methods and the actual operating behavior in the field, as well as the potential of filter testing which considers relevant RH variations.

2 Field Data from Gas Turbine Applications Serving as Reference Filters

Cassette filters returned from three different locations (UK, Spain, Germany) were analyzed. All three filters were used to clean the intake air of gas turbines under exposure to ambient air. They serve as reference point for the results obtained from the laboratory experiments. According to the operators, all filters showed normal behavior during operation. A summary of all available data on the respective filter elements is presented in Tab. 1.

Reference filter Z did not have a pre-filter installed during operation and, therefore, served as first filter stage. The absent pre-filter causes exposure to the coarse fraction as well as the fine fraction of the ambient aerosol. Compared to reference filters X and Y, which had pre-filters in place and served as second filter stage, this reflects in a much higher Δp increase over the course of operating time.

Scanning electron microscopy (SEM) images allow to evaluate the residual particle deposits on the reference filters. Filters were cut to 1-cm^2 samples and sputter-coated by a 4.5 nm thick palladium layer. A selection of images is presented in Fig. 1.

Table 1. Information on reference filters from gas turbine applications.

Type designation	Reference X	Reference Y	Reference Z
Filter material	Single-layer micro glasfiber, wetlaid, acrylate-based binder, hydrophobic	Single-layer micro glasfiber, wetlaid, acrylate-based binder, hydrophobic	Single-layer micro glasfiber, wetlaid, acrylate-based binder, hydrophobic
Material weight [$g\,m^{-2}$]	80–105	65–85	80–105
Material thickness [mm][a]	0.5–0.8	0.4–0.6	0.5–0.8
Initial differential pressure of the filter medium Δp_0 [Pa] (at 5.3 cm s^{-1})	30–50	55–75	25–45
Filter type	Rigid cassette filter	Rigid cassette filter	Rigid cassette filter
Pre-filter grade	ISO ePM10 50 %	ISO ePM10 60 %	No pre-filter installed
Operating location	UK, coastal area	Spain, coastal area	Germany, inland
Operating time t [h]	15 000	12 000	13 000
Final differential pressure increase of the filter element Δp [Pa] (at 4250 $m^3 h^{-1}$)	30	90	230

[a] Determined via microscopy without applied compression force.

Figure 1. SEM images of the upstream side, the cross-sectional area, and the downstream side of reference filters X, Y, and Z.

service life, by tailoring them to the actual operating conditions. One aspect is to generate an aerosol with the same PSD and solubility property, which is present during operation and therefore enabling a particle deposit structure based on the same mechanisms as typically seen in the field of application. The other aspect is the inclusion of defined RH variations typically found under ambient conditions.

Pei et al. discovered that RH is a major factor that affects particle deposition, while temperature is a minor factor [16]. The presence of RH is subject to change and reaches values up to 100 % depending on the location of the filter operation. This in turn can result in a change in composition of the aerosol, e.g., in terms of its PSD and the present states of matter. At low RH, salts in the ambient air remain solid, while at high RH they deliquescent, i.e., change their state of matter above their specific deliquescence relative humidity (DRH) from solid to liquid.

The influence of both aspects, PSD and RH, on the operating behavior of filters applied in the second and third filter stage of gas turbine plants and the resulting structures of particle deposits is considered in this study. Two sets of filter media are loaded with a test aerosol of relevant PSD according to the fine fraction of the ambient aerosol. One set is loaded at low RH of 30 ± 5 %, the other includes sequences of high RH between 85 % and 90 %. Subsequently, the results of both filter sets are compared to each other and to the previously described field data. To account for soluble particles in the atmosphere, while keeping the test matrix as simple as possible, a test aerosol with a fully soluble dispersed phase (KCl) is used in both sets of experiments. As most industry filters are exposed to a mix of soluble and insoluble particles during application, the experiments conducted here show an extreme case of the effect of elevated RH during filter operation, comparable with marine environments with very low concentrations of solid insoluble airborne particles, but mainly sea salt aerosol.

On the upstream side of each filter, all fibers show particle deposits (Fig. 1). Since filter Z did not have a pre-filter installed during operation, it was exposed to not only the fine fraction of the PSD of the ambient aerosol, but also to very large particles, sized 20 μm and more, which are clearly visible on the respective SEM image. Apart from these larger particles on filter Z, the deposits along the fibers of the upstream side of all filters are mainly shaped as large encrusted agglomerate structures. In rare cases, an intact dendrite structure is visible, as seen on the upstream side of reference filter Y (see enlarged insert in Fig. 1). Primary particle shapes are otherwise not distinguishable. A reduced number of particle deposits is visible throughout the cross-sectional of each filter. However, for filters X and Z, particle deposits are visible throughout the whole depth of the filters. On the downstream side of both filters, fewer, smaller particles remain, and (almost) no particles are visible on the downstream side of filter Y.

3 Instrumentation and Experimental Methods

3.1 Concept

This study suggests to modify the laboratory experiments, which are currently used to classify filters and estimate their

3.2 Filter Media

A variety of filter media can be implemented in the second or third stage of filter systems of gas turbines. Within the scope of this investigation, two high-efficiency glass fiber media were used as test filters. Test filter A is used in cassette filters classified at nominal operating conditions as ISO ePM1 80–85 % according to ISO 16890:2016. It is of similar material, which

reference filters X and Y are made of. Test filter B is employed for cassette filters achieving filter class E11 according to EN1822:2011. A pre-filter removes mainly coarse particles and is periodically replaced in intervals of 30 min. Further information on the aerosol generation and the application of the pre-filter can be found in the Supporting Information. Detailed specifications of each filter medium are listed in Tab. 2. Circular flat sheet filter samples with an effective area of 100 cm^2 are used in the experiments.

Table 2. Specification of flat sheet filter media used in laboratory test.

Type designation	Pre-filter	Test filter A[b]	Test filter B
Material	Polyolefine, meltblown, staple fiber	Single-layer micro glasfiber, wetlaid, acrylate-based binder, hydrophobic	Single-layer micro glasfiber, wetlaid, acrylate-based binder, hydrophobic
Weight [g m^{-2}]	175–225	80–105	80–105
Thickness [mm][a]	4–8	0.5–0.8	0.5–0.8
Differential pressure Δp_0 [Pa] (at 5.3 cm s^{-1})	40–60	50–70	150–180

[a] Determined via microscopy without applied compression force. [b] The filter medium is very similar to that of reference filters X und Y.

3.3 Filter Loading Procedures

Two sets of loading procedures are conducted in a commercial MFP 3000 HF (Palas$^®$) filter test rig, described in the Supporting Information. In both procedures the test filter is exposed to a KCl aerosol with a PSD resembling that of the fine fraction of the ambient aerosol. The particle generation including the corresponding PSD is described in the Supporting Information. The filter is exposed to a salt concentration of 4.68 mg m^{-3} (determined gravimetrically) at a constant face velocity of 8 cm s^{-1}, which corresponds to the face velocity of reference filters X, Y, and Z at nominal air flow rate. Throughout all experiments, a constant temperature of 23 °C is maintained.

The first procedure, in the following referred to as low-humidity procedure, includes the loading of the filter at constantly low 30 ± 5 % RH, well below the DRH of KCl (84.3 % at 25 °C [17]). During the low-humidity procedure, the filter is loaded up to a Δp of 400 Pa above Δp_0 of the clean filter (final total Δp = 560 Pa, filter A; Δp = 702 Pa, filter B). During the change of the pre-filter, the constant face velocity is maintained at 8 cm s^{-1}, while the particle generation is paused for approximately 120 s. Particle generation and filter loading resume after the new pre-filter is in place.

The second procedure, in the following referred to as humidity-cycles procedure, is a modified version of the first procedure and resembles the previously described test by Wilcox

et al. [14]. In the test procedure, moistening in cycles simulates the variances in the RH of the ambient air, e.g., due to fog, rain or condensation caused by day-night cycles. Droplets are likely separated by the inlet design of the filter system and pre-filter. Therefore, mainly the increased RH reaches the second and third stage. While aerosol composition and face velocity remain the same, variations in RH are added to the procedure. After one hour of particle loading at 30 % RH, the particle generation is stopped and the RH in the test rig is raised to 85 %. Over a period of 10 min, it is kept between 85 % and 90 %, before it is reduced back to 30 %. The exposure to elevated RH including the adjusting and stabilization of the respective RH takes approximately 30 min. Subsequently, the particle loading at 30 % RH is resumed. A 1-h particle loading paired with the following increase in RH and drying makes up one humidity cycle (Fig. 2). During the experiment, the pre-filter is again replaced every 30 min, including right before increasing the RH. No change of the pre-filter is required at the end of the humidity increase.
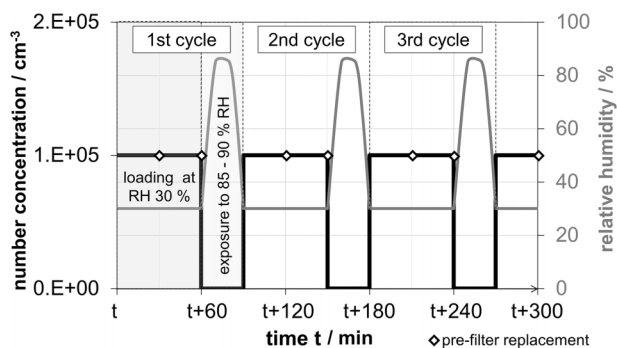
Figure 2. Excerpt of a time series of particle concentration and RH, to which the filter is exposed during the humidity-cycles procedure.

During the humidity-cycles procedure, each filter undergoes 35 humidity cycles. This includes controlled breaks at nighttime, during which temperature and RH in the test rig are maintained at 23 °C and 30 %, leaving for an overall active experimental time of over 50 h. A loading up to Δp = 400 Pa above Δp_0, such as performed during the low-humidity procedure, is not feasible, due to time constraints.

Both procedures are terminated with a final drying of the filter within the test rig with particle-free air at 10 % RH. After drying of the loaded filters, they are removed from the test rig. Prior to and following each experiment, their weight is measured, providing the particle load with a precision of ±1 mg. Finally, the filters are examined using SEM. For some filters the fractional separation efficiency was determined, by measuring the PSD of the test aerosol upstream and downstream of the filter with a U-SMSP (Palas$^®$) in the range of 0.02 to 0.78 μm at 30 % RH.

4 Results and Discussion

4.1 Comparison between Low-Humidity Procedure and Humidity-Cycles Procedure

4.1.1 Differential Pressure and Separation Efficiency

The two loading procedures lead to dissimilar Δp evolutions during particle loading (Fig. 3). Breaks in the loading process, as a result of replacing the pre-filter or cyclic increases in RH, were removed from Fig. 3 to show only the active loading time.
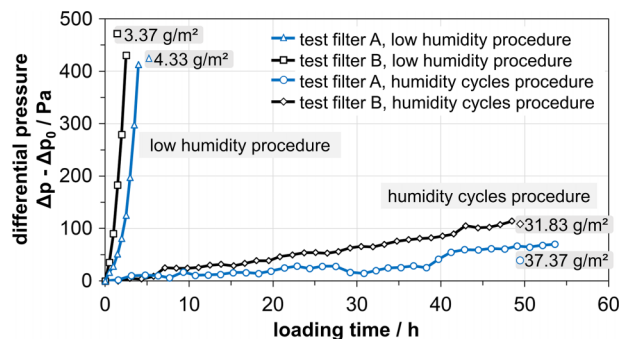
Figure 3. Differential pressure during particle loading of test filters A and B following the low-humidity and the humidity-cycles procedure, respectively.

During particle loading at 30 % RH according to the low-humidity procedure, both filters A and B reach their clogging point and the 400-Pa increase in Δp in less than 4 h. The increase in Δp of 400 Pa corresponds to particle loadings of 4.33 and 3.37 g m^{-2} for test filter A and B, respectively. For the humidity-cycles procedure, the Δp after each filtration cycle was recorded over time (Fig. 3).

In previous investigations by Schwarz et al. [18], a distinct representative development of the Δp was found during a single humidity cycle, starting with an increase during the first hour of a single cycle. The subsequent rise in RH leads to an instant decrease in Δp. Following this instant reduction, the Δp increases slowly with continued exposure to high RH and only decreases with the final drying of the filter. This distinct Δp evolution is exemplarily illustrated in Fig. 4 for the first and the final humidity cycle of test filter A.

Over the course of the whole experiment, the intermediate rise in Δp increases during the exposure to elevated RH with the number of filtration cycles. As the total amount of collected salt particles in the filter rises, more water is absorbed by the deposited salt. In turn, the increased amount of solution on the filter leads to the even higher intermediate rise in Δp. The exposure to high RH introduces two basic dynamic processes, dissolution of salt crystals, and recrystallization by drying. Sensible time parameters were chosen, which ensure that while keeping the procedure duration at a minimum, all basic dynamic processes are terminated in terms of their influence on the considered variables. During the phase of exposure to high RH this is reflected in the resulting Δp (Fig. 4). It reaches a local
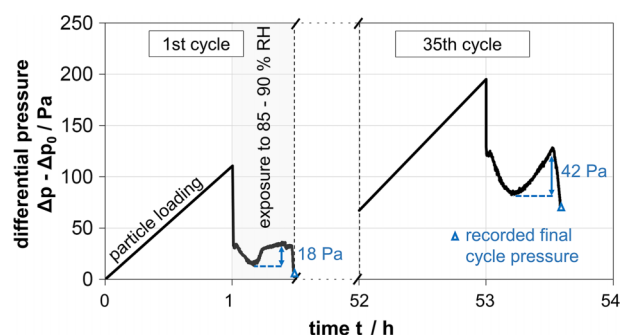
Figure 4. First and final humidity cycle of test filter A undergoing the humidity-cycles procedure with indicated increase in Δp during the exposure to high RH.

minimum. The subsequent rise in Δp indicates substantial liquid accumulation in the filter, which ensures that the salt fully dissolves. Based on previous investigations, the duration of drying likely leads to full recrystallization [18].

After the complete loading procedure, the mass loading is significantly higher after the humidity-cycles procedure relative to the low-humidity procedure, even though the final Δp remains significantly lower in comparison (Fig. 3). These results agree with previous studies investigating the effect of RH on the evolution of the Δp of depth filters loaded with soluble or insoluble particle materials [7–14].

A lower Δp of a filter applied in real-word applications may be interpreted as a beneficial sign for lower operating costs and a longer filter service life. However, the exposure to cycles of increased RH also influences the filter's fractional separation efficiency. As an example, the fractional separation efficiency of two flat sheet filter media A, after undergoing either the low-humidity procedure or the humidity-cycles procedure up to a mass loading of 4.33 g m^{-2}, was investigated. Despite the filters having the same mass loading, the humidity-cycles procedure results in a lower fractional separation efficiency than the low-humidity procedure in all size classes (Fig. 5).

The low-humidity procedure leads to a fractional separation efficiency above 98 % for all particle sizes, which clearly indicates clogging of the filter, while the humidity-cycles procedure
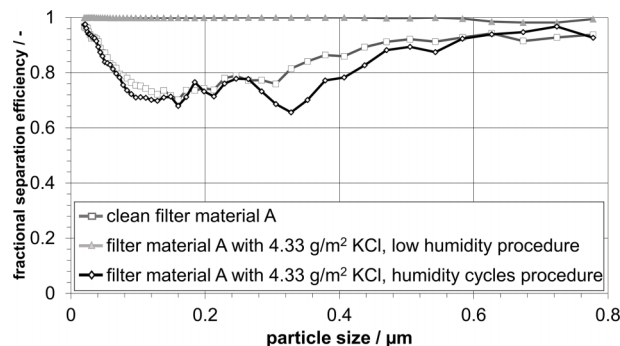
Figure 5. Fractional separation efficiency of filter medium A at a face velocity of 8 cm s^{-1} for the clean media, and with a particle load of 4.33 g m^{-2} after the low-humidity or the humidity-cycles procedure, respectively.

directs to a fractional separation efficiency, which closely resembles the initial efficiency of the clean filter. Therefore, a low increase in Δp rate during operation should be treated with caution, as the separation may not be as efficient as originally predicted by standard filter tests at constant moderate RH. Similar findings were reported by König et al. [19].

4.1.2 Analysis of Deposit Structures of the Test Filters

To obtain information about the particle deposit structures, samples of loaded test filters are examined with SEM. The upstream sides, cross-sectional areas, and downstream sides of all filters are analyzed (analogous to Fig. 1). The filters are removed from the test rig either before the clogging point for the low-humidity procedure (derived from the Δp evolution in Fig. 3, at $\Delta p = 80$ Pa and a mass loading of 2.3 g m^{-2}) or at the end of the loading process for humidity-cycles procedure (at $\Delta p = 70$ Pa and a mass loading of 37.4 g m^{-2}). Fig. 6 presents the SEM images of test filter A.

Following the low-humidity procedure, individual spherical particles form dendrite structures on the upstream side of the filter, which are starting to bridge the interstices between the fibers (Fig. 6a). Small particles are visible throughout the whole cross section of the filter (Fig. 6b). Particles on the downstream side of the filter are smaller and lower in number (Fig. 6c).

Following exposure to high RH during the humidity-cycles procedure, crystal structures up to 100 μm in diameter are attached to the fibers on the upstream side of the filter (Fig. 6 d). Here as well, particles are visible throughout the whole cross section (Fig. 6e). On the downstream side of the filter, the KCl also takes the characteristic cubic crystal shape (Fig. 6f). The crystals are much smaller than on the upstream side, where the majority of material is collected. The characteristic large cubic structures on both sides of the filter indicate that an increase in RH to 85–90 % over a short period of time impacts the shape and size of the deposited salt particles over the whole cross section of the filter media.

The SEM images provide an explanation for the previously observed higher mass loading at lower overall Δp for filters

exposed to high RH during humidity cycles (Sect. 4.1.1). During the loading at low humidity, dendrite structures form on the filter quickly covering the cross sections between fibers on the upstream side of the filter. During exposure to RH between 85 % and 90 % these expansive dendrite structures collapse due to partial or full dissolving of the KCl. Upon drying, compact crystal structures form on the fibers (Fig. 6d). This reduction in surface area of the particle deposits leaves large sections of the filter unloaded and free for the aerosol to pass through, which in turn leads to the observed low Δp and decline in separation efficiency. In other words, at almost the same Δp (here ≈ 80 Pa) the filter with exposure to higher humidity has a substantially higher mass loading (here by a factor of 16). An analysis of the SEM images of test filter B is provided in the Supporting Information and leads to similar conclusions.

4.2 Comparison between Laboratory and Field Data

The obtained results from the laboratory experiments are compared to the analyzed field data. Since information on the reference filters is limited to Δp increase, operating hours, and general filter media information, while exposure conditions such as particle concentration, humidity, and mass loading cannot be estimated sufficiently, a direct quantitative comparison is not possible. Therefore, the particle deposits were analyzed by SEM and compared. As previously discussed, all three reference filters returned from industry showed crust deposition on their fibers, especially on the upstream side of the filter (Fig. 1). A comparison between SEM images of the upstream side of reference filter X with laboratory filters from a similar material (filter A) indicates the different particle deposit structures after the loading procedures (Fig. 7). Additionally, all reference filters were analyzed by means of energy dispersive X-ray spectroscopy (EDX). Exemplarily, the results of the EDX analysis of the upstream side of reference filter X are presented in Fig. 7.

Fig. 7a presents reference filter X returned from coastal UK aged in a gas turbine plant, Fig. 7b test filter A after undergoing the low-humidity procedure, and Fig. 7c test filter A after undergoing the humidity-cycles procedure. The material collected in the industrial application is compact with no intact dendrite structures and few primary particles visible (Fig. 7a). In the lab test without exposure to high humidity, primary particles of soluble material can be identified following the low-humidity procedure and dendrite structures remain fully intact (Fig. 7b). On the other hand, the exposure to humidity cycles leads the KCl to form large crystals (Fig. 7c) and results in much more compact deposit structures than exposure to solely low RH does.
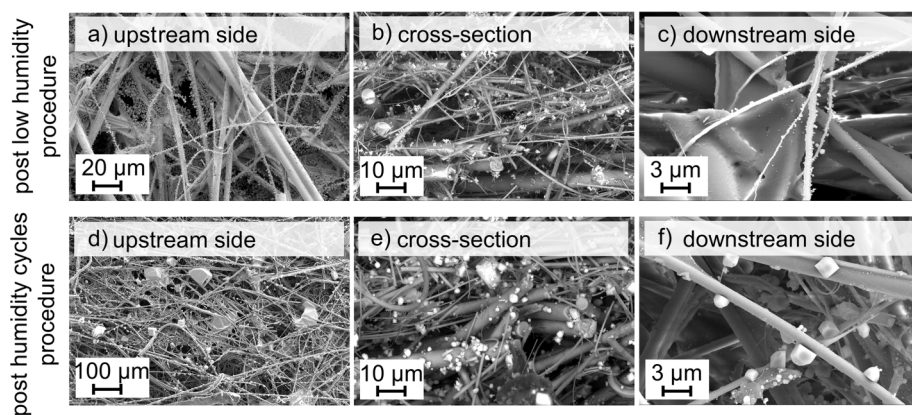
Figure 6. SEM images of test filter A after undergoing the low-humidity procedure of the (a) upstream side, (b) center of the cross section, (c) downstream side and after undergoing the humidity-cycles procedure of the (d) upstream side, (e) center of the cross section and (f) downstream side.

Comparing the three images, dendrite structures remain only intact, when the filter is loaded at low RH, here 30 % and never exposed to increased levels of RH above DRH. Exposure to elevated RH during humidity cycles or as natural occurring variations in real-world applications leads to more compact structures and crusts. Therefore, the filter following the low-humidity procedure does not lead to particle deposits as seen on the reference filter from gas turbine application. Differences between the filter loading according to the humidity-cycles procedure and reference filter X remain, since no clear particle structures and crystals are visible on the SEM images of the reference filter. This is likely due to a different chemical composition of the particle deposits. Unlike the test filters loaded under laboratory conditions, the reference filters have likely not been exclusively exposed to soluble materials, since ambient aerosol contains a mix of soluble and insoluble particles [20]. Therefore, the SEM image of reference filter X (Fig. 7a) does not show clear cubic particle deposit structures.

The EDX analysis of reference filter X (Fig. 7d) confirms this thesis by providing additional information on the type of particles that were collected during filter operation in the gas turbine plant. Mainly various alkali and alkaline earth metals (Na, K, Ca, Ba, Mg) as well as iron, oxygen, aluminum, chlorine, and sulfur are detected. These elements can be present as insoluble oxides (Fe, Al, Si + O) and/or soluble chlorides and sulfates (Na, K, Mg, Ca + Cl/+ S and O). There is thus strong reason to presume that the filters were exposed to a mix of soluble and insoluble components. In accordance with the results presented for reference filter X, the EDX analysis of all other reference filters indicate similar results.
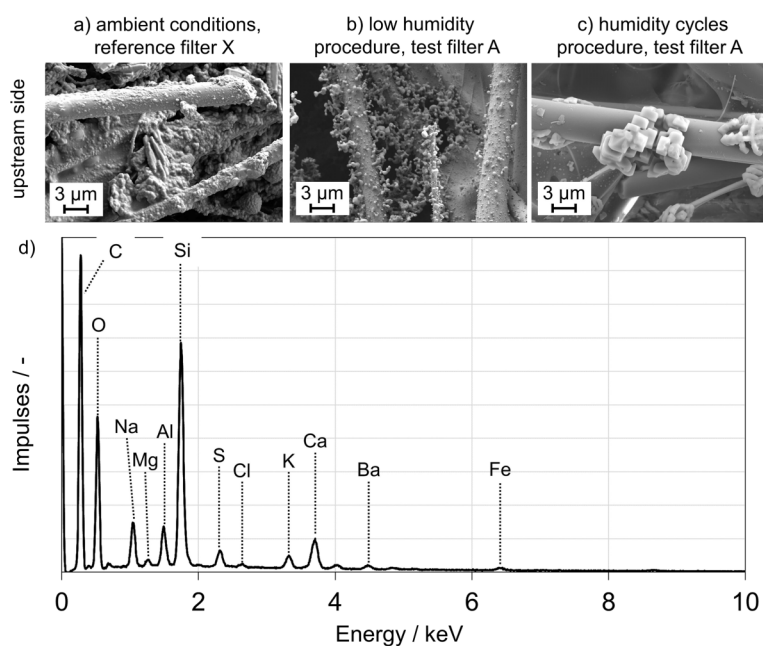
5   Conclusion and Outlook

To more accurately reproduce real-world operating conditions in filter tests, a test aerosol with specific PSD was developed, which reproduces the fine fraction of the ambient aerosol, seen in the second and third filter stage of turbine cleaning systems. Two sets of experiments were conducted with this test aerosol: one included loading of filters with soluble KCl at low RH of 30 % (low-humidity procedure), the other included additional periodical exposure to RH between 85 % and 90 % (humidity-cycles procedure), simulating natural variations in RH in the ambient air. The resulting deposit structures were directly compared to three analyzed industry samples, which were applied in gas turbine plants in three different representative locations.

The experiments conducted with periodical exposure to high RH show a much lower Δp increase rate than filters loaded according to the low-humidity procedure at 30 % RH. SEM images demonstrated that, compared to a low-humidity procedure, the exposure to humidity cycles leads to a more compact particle deposit structure. Covering less filter surface area, it results in the previously discussed lower increase rate in the Δp. In addition to a lower rate of increase in Δp due to exposure to high RH, which may seem beneficial regarding operating costs, the increase in free surface area also causes a decrease in the separation efficiency of the filter.

Overall, the results confirm that typical filter testing at constant reference humidity below DRH, as testing standards such as ISO 16890 suggest, does neither lead to Δp increase rates nor to particle deposit structures seen in industrial applications. It is therefore not a credible foundation for a reliable service life prediction of such filters. To predict the service life of air filters more accurately and reliably based on laboratory tests, this study suggests to develop new standard procedures for laboratory testing considering the PSD of the aerosol and the RH to which the filter is exposed during operation. Other factors such as the effect of the particle material containing both soluble and insoluble particles or of liquid droplets or saltwater spray in the process gas are also of interest and will be investigated in future studies.

Supporting Information

Supporting Information for this article can be found under DOI: https://doi.org/10.1002/ceat.202100344.

Figure 7. SEM images of the upstream side of the same type of filter medium loaded under different conditions: (a) industry filter X loaded in a gas turbine plant, (b) test filter A after low-humidity procedure, (c) test filter A after humidity-cycles procedure, and (d) EDX analysis of the upstream side of reference filter X.

Symbols used

DRH	[–]	deliquescence relative humidity
Δp	[Pa]	differential pressure
RH	[–]	relative humidity
t	[min, h]	time

Abbreviations

EDX	energy dispersive X-ray spectroscopy
PSD	particle size distribution
SEM	scanning electron microscopy

References

[1] DIN EN ISO 29461, *Air Intake Systems for Rotary Machinery – Test Methods*, Beuth, Berlin **2020**.

[2] DIN EN ISO 16890, *Air Filters for General Ventilation*, Beuth, Berlin **2017**.

[3] DIN EN ISO 29463, *High-Efficiency Filters and Filter Media for Removing Particles in Air*, Beuth, Berlin **2019**.

[4] DIN EN ISO 16890-1, *Air Filters for General Ventilation*, Beuth, Berlin **2017**.

[5] P. Weber, Service Life Calculation of Multistage Filter Systems, *M.Eng. Thesis*, Duale Hochschule Baden-Württemberg, Stuttgart **2019**.

[6] DIN EN ISO 15957, *Test Dusts for Evaluating Air Cleaning Equipment*, Beuth, Berlin **2015**.

[7] A. Gupta, V. J. Novick, P. Biswas, P. R. Monson, *Aerosol Sci. Technol.* **1993**, *19 (1)*, 94–107. DOI: https://doi.org/10.1080/02786829308959624

[8] A. Joubert, J. C. Laborde, L. Bouilloux, S. Callé-Chazelet, D. Thomas, *Aerosol. Sci. Technol.* **2010**, *44 (12)*, 1065–1076. DOI: https://doi.org/10.1080/02786826.2010.510154

[9] A. Joubert, J. C. Laborde, L. Bouilloux, S. Chazelet, D. Thomas, *Chem. Eng. J.* **2011**, *166 (2)*, 616–623. DOI: https://doi.org/10.1016/j.cej.2010.11.033

[10] Q. Ribeyre, A. Charvet, C. Vallières, D. Thomas, *Chem. Eng. Sci.* **2017**, *161*, 109–116. DOI: https://doi.org/10.1016/j.ces.2016.12.013

[11] A. F. Miguel, *J. Aerosol Sci.* **2003**, *34 (6)*, 783–799. DOI: https://doi.org/10.1016/S0021-8502(03)00027-2

[12] J. F. Montgomery, S. N. Rogak, S. I. Green, Y. You, A. K. Bertram, *Environ. Sci. Technol.* **2015**, *49 (20)*, 12054–12061. DOI: https://doi.org/10.1021/acs.est.5b03157

[13] J. F. Montgomery, S. I. Green, S. N. Rogak, *Aerosol Sci. Technol.* **2015**, *49 (5)*, 322–331. DOI: https://doi.org/10.1080/02786826.2015.1026433

[14] C. Pei, Q. Ou, D. Y. H. Pui, *Sep. Purif. Technol.* **2019**, *212*, 75–83. DOI: https://doi.org/10.1016/j.seppur.2018.11.009

[15] *Proc. of the ASME Turbo Expo* (Eds: M. Wilcox, R. Kurz, N. Poerner, K. Brun), The American Society of Mechanical Engineers, New York **2012**.

[16] C. Pei, Q. Ou, D. Y. H. Pui, *Sep. Purif. Technol.* **2021**, *255*, 117679. DOI: https://doi.org/10.1016/j.seppur.2020.117679

[17] I. N. Tang, in *Aerosol Chemical Processes in the Environment* (Ed: K. R. Spurny), CRC Press, Boca Raton, FL **2000**, Ch. 4, 61–80.

[18] A. D. Schwarz, J. Meyer, A. Dittler, *Sep. Purif. Technol.* **2021**, *259*, 118128. DOI: https://doi.org/10.1016/j.seppur.2020.118128

[19] C. König, F. Schmidt, T. Engelke, *Chem. Ing. Tech.* **2018**, *90 (7)*, 1005–1010. DOI: https://doi.org/10.1002/cite.201700012

[20] www.dwd.de/EN/research/observing_atmosphere/composition_atmosphere/aerosol/cont_nav/chemical_composition_of_aerosols_node.html (Accessed on June 10, 2021)